small methods

www.small-methods.com

Strep-Tag II and Monovalent *Strep*-Tactin as Novel Handles in Single-Molecule Cut-and-Paste

*Katherine R. Erlich, Fabian Baumann, Diana A. Pippig, and Hermann E. Gaub**

Directed spatial assembly of single molecules on a surface presents an opportunity to precisely control the positioning, density, and geometry of molecules of interest within an ensemble. In contrast to bulk averaging, this enables detection and analysis of individual behavior within such a designed ensemble. The atomic force microscopy (AFM)-based technique of single-molecule cut-and-paste (SMC&P) facilitates the arrangement of a variety of biomolecules on a surface through different handling strategies. This technique requires cantilever- and surface-handles that simultaneously adhere to a prerequisite rupture force hierarchy, and also do not cross-interact with each other or the transported molecules. As the molecules of interest diversify, so too must the handling methods to accommodate their unique characteristics. Here, it is demonstrated that a previously developed monovalent variant of *Strep*-Tactin and its corresponding *Strep*-Tag II peptide ligand comprise a viable cantilever handling complex for SMC&P. Ultimately, this expansion to the SMC&P toolbox increases the system's versatility for new molecules of interest yet to be studied.

The frontier of nanoscale studies frequently presents unexpected challenges that must be overcome with innovation. As such, universally applicable approaches often do not exist, and instead diverse methods or tools must be developed. Bottom-up synthetic biology employs fundamental biological components as the building blocks for artificial biological systems with novel characteristics. A major endeavor of this broad field is to develop unique molecular-organization techniques, such as engineered protein modules[1] and enzyme cascades assembled on DNA-origami scaffolds.[2] Single-molecule cut-and-paste (SMC&P) is one such organization technique, merging bottom-up assembly with control on the level of single molecules. SMC&P utilizes the single-molecule force spectroscopy (SMFS) and lateral surface positioning of atomic force microscopy (AFM)[3–5] to deposit molecules of interest in arbitrary patterns on a functionalized glass surface with nanometer-precision. There exist several key challenges in SMFS that are constantly improved upon: signal-to-noise limits of data resolution, and specific handling. Advances in existing tools, such as modified cantilevers in AFM-based SMFS,[6] can greatly improve data quality and expose previously inaccessible levels of detail. Precise and versatile control of molecules of interest can likewise open up new avenues of study. For example, protein-labeled DNA-tethering strategies in optical-tweezers experiments offer additional flexibility in handling biomolecules for mechanical measurements.[7] Similarly, SMC&P requires robust immobilization and handling schemes for the specific and controlled arrangement of diverse biological agents. With a more expansive repertoire of handling strategies, its components could potentially be tailored to enable arrangement of any molecule of interest in a well-defined orientation.

During each SMC&P cycle, a noncovalently immobilized transfer molecule of interest is picked up from a depot area via a cantilever-coupled affinity handle. The cantilever relocates the transfer molecule to a target area, where it then deposits said molecule and is recycled back to the depot area to repeat the process. Arrays of molecules are assembled with precise localization in the target area, where their properties such as their fluorescent behavior in an ensemble or as individuals can be analyzed. For example, hybrid DNA–RNA molecules were specifically arranged and immobilized on a surface via complementary oligonucleotides. The resulting duplexes formed aptamers that stabilized the structure of a target dye molecule, enabling it to produce a fluorescent signal upon binding the SMC&P-arranged constructs.[8] Proteins have also been integrated into SMC&P, including constructs containing modified green fluorescent protein (GFP)[9] with different surface-immobilization strategies and a protein-based handle for the cantilever.[10,11] Directed placement of molecules within the nanoapertures of zero-mode waveguides with SMC&P is also possible. These nanoapertures facilitate measurements in a confined volume and improve background fluorescence when compared to conventional fluorescence microscopy. Importantly, the precise placement of molecules via SMC&P decreases the heterogeneity of fluorescence intensity and lifetime that results from stochastic immobilization and quenching effects from the metallic sidewalls.[12] In combination with fluorescence microscopy, SMC&P therefore presents new opportunities to examine biomolecular behavior on the single-molecule level with precise control of surface location and environment.

SMC&P fundamentally relies on a hierarchy of rupture forces of the specific interactions between the transfer molecule and the depot area (F_D), the cantilever (F_C), and the target area

K. R. Erlich, Dr. F. Baumann, Dr. D. A. Pippig, Prof. H. E. Gaub
Center for NanoScience and Department of Physics
Ludwig Maximilians University of Munich
Amalienstraße 54, 80799 Munich, Germany
E-mail: gaub@lmu.de

DOI: 10.1002/smtd.201700169

(F_T) such that $F_D < F_C < F_T$. Consequently, this system demands a palette of selective immobilization and pickup methods so that the forces involved are tunable to fit this hierarchy. Furthermore, an ideal SMC&P scheme uses orthogonal agents that avoid unwanted cross-reactivity. Even small peptide tags and single-stranded DNA anchors could have adverse interactions between themselves or with molecules of interest, which in turn could interfere with SMC&P efficiency or molecule behavior. Therefore, a modular approach to construct design confers a degree of plasticity and promotes integration of any molecule of interest into SMC&P. By expanding the selection of cantilever- or surface-handles, the system can be further adapted to specific force and mechanistic requirements.

Strep-Tactin, an engineered variant of streptavidin, is a tetravalent complex that specifically binds with high affinity to the short peptide *Strep*-tag II (SII).[13] A monovalent version of *Strep*-Tactin (monoST) was recently developed and implemented in SMFS as a cantilever-immobilized handle for protein constructs harboring an SII-peptide.[14] The rupture forces of SII:monoST were found to be dependent on loading rate as well as location of SII in the protein construct, with N-terminal SII resulting in much lower rupture forces than C-terminal SII under identical loading rates. Its tethering geometry-dependent force regime and tunable rupture forces make the SII:monoST complex a compelling candidate as a handling system for SMC&P. Moreover, its addition to the growing SMC&P toolbox advances the technique toward the ultimate goal of enabling precise arrangement of any molecule of interest.

A construct consisting of GFP with an N-terminal SII and a C-terminal ybbR tag was previously expressed and purified, and it was also demonstrated in SMFS that the rupture forces of an N-terminal SII and monoST were lower than the force required to unfold GFP.[14] This construct was here employed in SMC&P, where the relatively low rupture forces of N-terminal SII and monoST were advantageous for preserving the fold and thus fluorescence of GFP during the transport process. The C-terminal ybbR tag was covalently modified with 3′-coenzyme A (CoA) single-stranded DNA by the phosphopantetheinyl transferase enzyme Sfp synthase.[15] Hybridization of the DNA anchor to a complementary DNA strand in either zipper- or shear-orientation enabled noncovalent surface immobilization to the depot and target areas, respectively (**Figure 1**a).

SMC&P was executed in a custom-built hybrid AFM/total-internal-reflection fluorescence microscopy (TIRFM) instrument.[16] Chimeric transfer constructs were picked up from the depot area via a monoST-coupled cantilever and deposited into the target area over 395 consecutive SMC&P cycles. The technique utilizes a hierarchy of rupture forces between the transfer molecule and the depot storage molecule (F_D), the cantilever handle (F_C), and the target storage molecule (F_T) such that $F_D < F_C < F_T$. The rupture forces of DNA duplexes are tuned via duplex length and pulling geometry (zipper vs shear).[17] Additionally, the rupture forces of protein–protein interactions are influenced by loading rates.[14,18,19] In this way, it is possible to optimize a scheme to consistently transport transfer constructs and regenerate the cantilever (Figure 1b).

The distinct behaviors of the depot DNA duplex and the SII:monoST complex upon unbinding and rupture are illustrated in their respective force curve patterns (**Figure 2**). When pulled apart in zipper orientation, the basepair-by-basepair

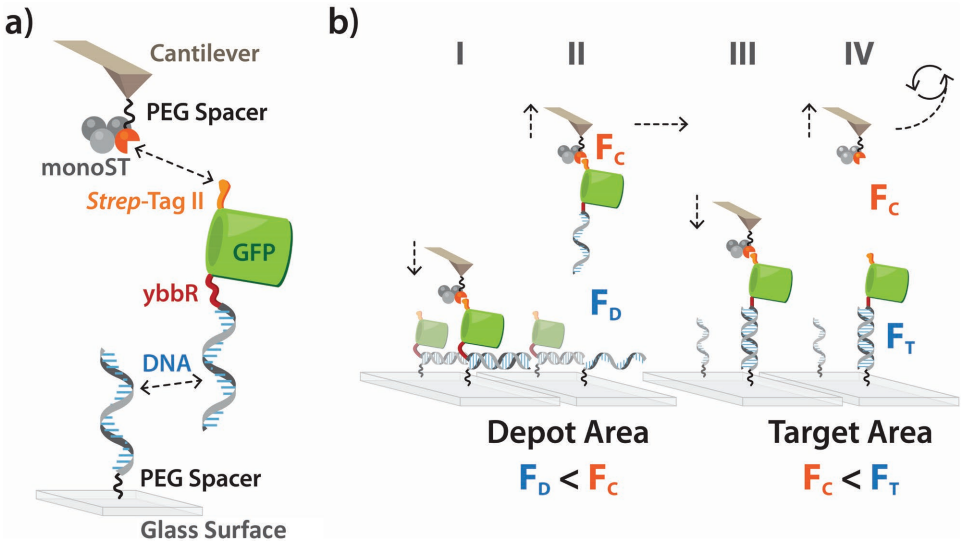

Figure 1. Monovalent *Strep*-Tactin and the GFP transfer construct employed in SMC&P. a) The chimeric transfer construct consists of a GFP molecule with an N-terminal SII as well as a C-terminal ybbR tag, which is then covalently coupled to 3′-CoA single-stranded DNA via reaction catalyzed by Sfp synthase. The DNA anchor binds noncovalently to the surface via a complementary DNA strand. The cantilever is covalently coupled to the single functional subunit of monoST, which targets SII of the transfer construct. b) Repeatable transfer cycling of SMC&P depends on a force hierarchy determined by DNA hybridization geometry and the SII:monoST interaction. The cantilever approaches the depot surface, and monoST binds to SII of a transfer molecule immobilized via complementary DNA in zipper orientation (I). The cantilever retracts and removes the transfer molecule as the DNA unzips (II). The cantilever then transports the transfer molecule to the target surface where the transfer molecule binds to complementary DNA in shear orientation (III). Retraction of the cantilever ruptures the SII:monoST complex, and the cantilever is recycled back to the depot area to repeat the process (IV). The rupture forces of the transfer construct with the DNA in the depot area (F_D), monoST on the cantilever (F_C) and DNA in the target area (F_T) are tuned such that $F_D < F_C < F_T$.

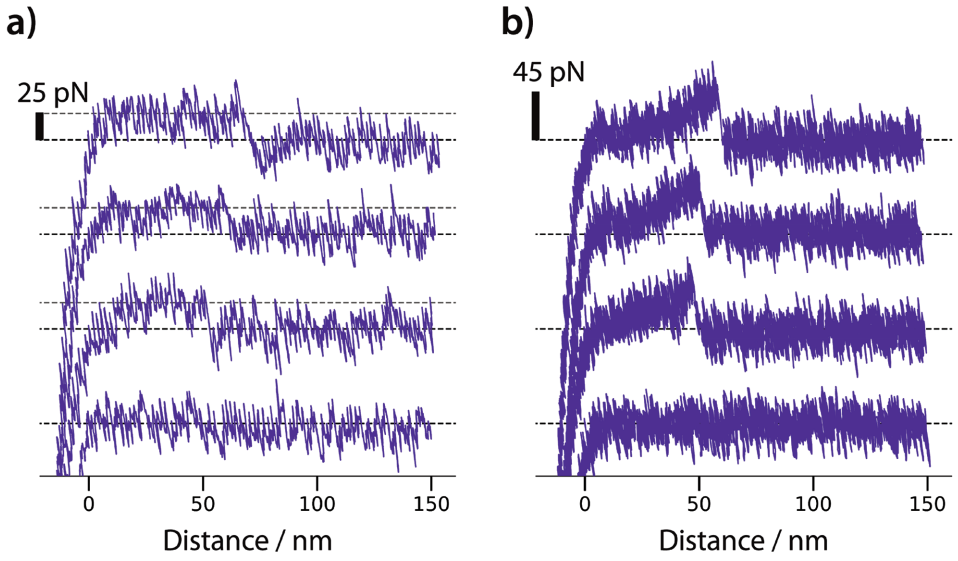

Figure 2. a,b) Typical force–distance curves of single-molecule depot pickup (a) and target deposition events (b). Depot pickup events occur when the transfer construct-surface DNA complex is unzipped, resulting in a plateau of relatively constant force at ≈25 pN (depicted by the dashed gray lines). Target deposition events occur when the newly established transfer construct–surface DNA complex in shear orientation remains intact, and instead the SII:monoST complex unbinds. This results in a gradual buildup of force and a sharp unbinding peak at ≈45 pN. In some cases, no molecules were picked up or deposited, which is reflected in the zero-force curves (bottom-most traces). The baseline for each curve of 0 pN force is depicted by the dashed black lines.

unzipping of DNA is described quantitatively by an equilibrium thermodynamic model,[20,21] leading to a plateau of constant force. During a pickup event from the depot area, the 40 bp DNA duplex melts at ≈25 pN, which is consistent with previous SMC&P experiments using this same DNA duplex.[10,11] The non-equilibrium unbinding of the SII:monoST interaction occurs at forces significantly greater than this value at the given loading rates.[14] Consequently, the transfer-depot DNA duplex melts while the SII:monoST bond stays intact, allowing for consistent pickup of molecules from the depot. The transfer construct is then transported to the target area where it binds to the surface-immobilized target DNA in shear orientation. The geometry of the 40 bp DNA duplex confers a substantial increase in rupture force due to force propagation through all basepairs (a most probable unbinding force of ≈65 pN at the observed loading rates around 300 pN s^{-1}).[22] Meanwhile, the SII:monoST complex ruptures in a non-equilibrium process at ≈45 pN at this pulling speed and apparent loading rate. Thus, the transfer construct detaches from the cantilever upon retraction and remains deposited in the target area. The cantilever-coupled monoST complex is now free to pick up a new transfer construct in repeated SMC&P cycles. This therefore presents the opportunity to carefully tune the expected rupture force of a protein-based handle by varying the loading rate, while simultaneously incurring minimal or no effect on the expected rupture force of a DNA-based tether. Hence, the SMC&P force hierarchy can be further reinforced by adjusting the pulling speed in each step of the cycle to maximize the difference in rupture force of the cantilever handle and surface tether. Examples of single-molecule pickup and deposition events demonstrate the plateau-like force curves observed from basepair-by-basepair unzipping of DNA in the depot area (Figure 2a) and the worm-like chain (WLC)[23] stretching behavior of the poly(ethylene glycol) (PEG) linkers followed by a sharp unbinding peak of the SII:monoST complex in the target area (Figure 2b). Notably, no additional force barriers are observed, which is consistent with the GFP and *Strep*-Tactin fold staying intact throughout the transfer process.

Following completion of the SMC&P sequence, the GFP-containing transfer molecules arranged in a dinosaur pattern were imaged by TIRFM (**Figure 3**), producing a clearly discernible outline. The previously demonstrated longevity of the monoST complex after hundreds of pulling events[14] is confirmed here with successful SMC&P transport over 395 consecutive cycles. Moreover, the rupture forces exhibited by the SII:monoST complex are in a range that is compatible with the well-characterized depot-transfer and target-transfer DNA duplex unbinding. Patchiness in the pattern can be partially attributed to the limited photostability of GFP, likely causing a fraction of the transfer molecules to photobleach during purification and experimental setup before imaging. There are also cases where a cycle fails to transport a transfer construct, as SMC&P and the underlying rupture forces are probability-dependent. Surface defects and densities can also influence the efficiency of SMC&P. However, the corresponding force–distance curves in every cycle can control for this; an inherently nonfluorescent or bleached transfer construct produces a deposition force curve but no fluorescence signal, and a failed transport cycle produces neither (e.g., the bottom-most force traces in Figure 2). Such analysis was previously executed by Pippig et al. to evaluate a widely spaced grid pattern of individual GFP molecules deposited by SMC&P.[11] The same strategy could conceivably be applied to any SMC&P experiment in which it is necessary to determine exactly which deposition points contain the transported molecules of interest.

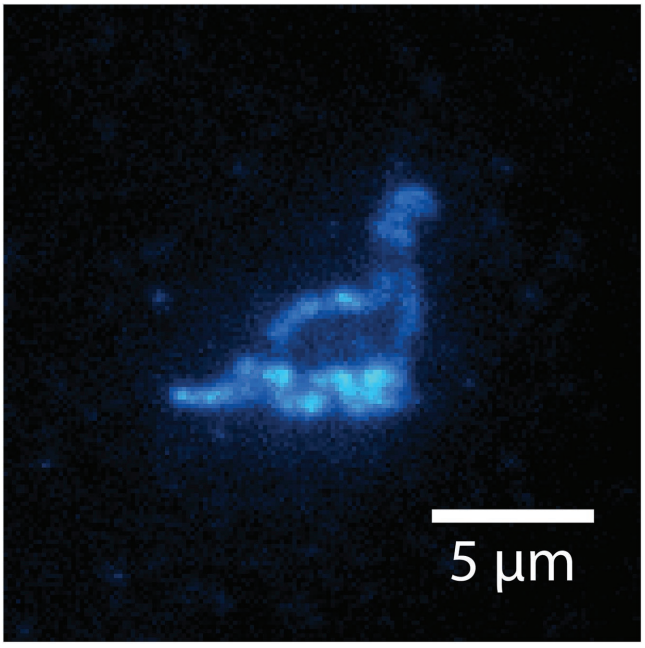

Figure 3. TIRFM image of GFP molecules after SMC&P in a dinosaur pattern. The image is composed of the average pixel intensity of 30 stacked frames from TIRFM acquisition (0.12 s exposure time at ≈10 W cm^{-2}) with a blue laser. The pattern consists of 395 deposited molecules spaced 150 nm apart.

SMC&P is an attractive strategy for the study of enzyme activity, as it enables precise placement of molecules of interest on a surface with known positioning, in contrast to stochastic surface immobilization. Moreover, the pattern of molecules to be arranged is completely arbitrary, allowing unrestricted pattern design for the investigation of the effects of relative geometry within networks or clusters of enzymes. Single-molecule enzyme analyses may prove to be indispensable for gaining new insights into the dynamic nature of enzyme networks, such as cellulosomes. These cellulose-degrading complexes are utilized by many species of cellulolytic bacteria, and have the critical characteristic that cellulase enzymes are strategically arranged on a scaffold to increase the efficiency of the catalytic network.[24,25] As the spatial organization of the enzymes is a key part of their function in vivo, similarly taking into account their relative geometry could provide new understanding of the cellulosomal components on a single-molecule level. Therefore, SMC&P may be an advantageous strategy for directed arrangement and investigation of this enzyme network.

Identification of diverse surface-immobilization methods is likewise a prerequisite for SMC&P's versatility. An intriguing potential use of the SII:monoST complex in SMC&P would leverage its terminus-dependent rupture force regimes to create SII-harboring depot and target regions. A monoST-containing transfer construct could be transported from the N-terminal SII depot (lower rupture forces) to the C-terminal SII target (higher rupture forces) via a cantilever tag of some intermediate rupture force. This presents an opportunity to forego DNA-based anchoring systems, which could be crucial for studying DNA-binding enzymes such as polymerases or ligases.

We have demonstrated that the SII:monoST complex is a viable handle for SMC&P. Although this study serves mainly as a proof of concept, it is invaluable to the expansion of SMC&P that diverse immobilization and cantilever handling options are available. Arrangement of molecules that perform biological functions—such as enzymes or aptamers—requires careful consideration of the unique properties, requirements or limitations of each molecule of interest. Unexpected secondary interactions between a tethering system and an enzyme could hinder SMC&P transport or interfere with enzymatic activity. In other words, it is possible that universal means of surface immobilization or cantilever handling may ultimately not exist. It is therefore advantageous to have a modular system with exchangeable components so that no molecule of interest must be excluded from study. With the addition of the SII:monoST handle system to the SMC&P toolbox, we have expanded the handling options available and given this technique a new degree of flexibility.

Experimental Section

Detailed information on all sections can be found in the Supporting Information.

Preparation of Monovalent Strep-Tactin: A heterotetrameric monovalent version of *Strep*-Tactin (monoST) was designed, expressed, purified, and reconstituted as previously described by Baumann et al.[14] In brief, the nonfunctional subunits and the single functional subunit harboring a 6×His tag and a reactive Cysteine residue were separately expressed in *Escherichia coli* (*E. coli*) BL21(DE3)-CodonPlus cells. Inclusion bodies were dissolved and denatured, and the dissolved inclusion body fractions of the nonfunctional and functional subunits were mixed in a ratio of 10:1, respectively. Subunits were refolded by slowly and dropwise adding to a reservoir of 1× phosphate-buffered saline (PBS). The assembled monoST was purified by Ni-IMAC affinity chromatography. The fractions containing monoST were isolated and dialyzed against 1× PBS. Purified monoST was long-term stored at 4 °C in the presence of tris(2-carboxyethyl)phosphine (TCEP) beads.

Preparation of Superfolder Green Fluorescent Protein (sfGFP) Construct and DNA Coupling: An sfGFP[9] transfer construct was designed, expressed, and purified as previously described by Baumann et al.[14] In brief, the construct harbors an N-terminal *Strep*-tag II (SAWSHPQFEK = SII)[13] and a C-terminal ybbR-tag (DSLEFIASKLA)[15,26] to enable specific cantilever handling and DNA coupling, respectively. The GFP gene was cloned into a modified pET28a vector that contains an N-terminal 6×His-tag followed by a PreScission Protease cleavage site (PreSc). The resulting fusion protein (6×His-PreSc-SII-sfGFP-ybbR) was expressed in *E. coli* BL21(DE3)-CodonPlus cells. The sfGFP construct was obtained in the soluble fraction after cell lysis and purified by Ni-IMAC affinity chromatography. Selected fractions of purified protein were then dialyzed overnight against storage buffer (50×10^{-3} M Tris HCl pH 7.5, 150×10^{-3} M NaCl, 2×10^{-3} M dithiothreitol (DTT), 5% glycerol) and stored long-term at −80 °C. The sfGFP construct was covalently coupled to DNA via the enzyme Sfp transferase as similarly described by Pippig et al.,[11] which is slightly altered from the protocol of Yin et al.[26] PreScission Protease, Sfp transferase, and CoA-modified transfer DNA (biomers.net GmbH, Ulm, Germany) were incubated with the purified 6×His-PreSc-SII-sfGFP-ybbR construct at room temperature for 2 h for simultaneous cleavage of the 6×His tag and covalent coupling of the ybbR tag to DNA. The reaction was filtered and then stored on ice until application in a microfluidic system.

Preparation of Cantilevers: MLCT cantilevers (Bruker, Camarillo, USA) were silanized in 3-(aminopropyl)dimethylethoxysilane and subsequently functionalized with a hetero-bifunctional PEG crosslinker[27,28] with *N*-hydroxy succinimide and maleimide groups (MW 5000). Cantilevers were covalently coupled to monoST.

Preparation of Glass Surfaces: Glass cover slips were silanized in (3-aminopropyl)dimethylethoxysilane and subsequently functionalized with a hetero-bifunctional PEG crosslinker with *N*-hydroxy succinimide and maleimide groups (MW 5000). Thiol-modified Depot and Target DNA was reduced and then purified by ethanol precipitation. A poly(dimethylsiloxane) (PDMS) microfluidic system—based on the system described by Kufer et al.[17]—was fixed on the PEGylated cover glass. Depot and Target channels were functionalized with their respective reduced DNA, and the sfGFP-DNA chimera construct was incubated in the Depot channel for 1 h. The Depot channel was then flushed with 1× PBS to remove unbound- or nonspecifically bound sfGFP. The microfluidic system was then removed and the surface submerged in 1× PBS.

AFM/TIRFM Measurements: SMC&P experiments were carried out on a combined AFM/TIRFM setup, as described previously.[16] The dinosaur pattern was written in 395 transfer cycles with 150 nm spacing between each deposition point. The pulling speed in the depot was set to 2 μm s^{-1} and in the target to 0.2 μm s^{-1}. Rupture forces and loading rates were evaluated from AFM force–distance curves that were recorded for each pickup and deposition process utilizing a quantum mechanically corrected WLC model.[29] Blue laser excitation at 488 nm with an estimated intensity of ≈10 W cm^{-2} was utilized to monitor the GFP fluorescence. Fluorescent images were evaluated and processed with the analysis software ImageJ.

Supporting Information

Supporting Information is available from the Wiley Online Library or from the author.

Acknowledgements

This work was supported by the European Research Council (Cellufuel, Advanced Grant No. 294438) and the German Research Foundation (SFB 1032-A01). The authors thank Ellis Durner and Markus A. Jobst for AFM/TIRFM hardware and software support; Angelika Kardinal and Thomas Nicolaus for laboratory support; and Christoph Hohmann of Nanosystems Initiative Munich (NIM) for graphic design assistance and production.

Conflict of Interest

The authors declare no conflict of interest.

Keywords

AFM, monovalent *Strep*-Tactin, single-molecule cut-and-paste, single-molecule fluorescence, spatial arrangement

Received: April 27, 2017
Revised: May 13, 2017
Published online:

[1] S. Hirschi, M. Stauffer, D. Harder, D. J. Müller, W. Meier, D. Fotiadis, *Chimia* **2016**, *70*, 398.
[2] A. Rajendran, E. Nakata, S. Nakano, T. Morii, *ChemBioChem* **2017**, *18*, 696.
[3] G. Binnig, C. F. Quate, C. Gerber, *Phys. Rev. Lett.* **1986**, *56*, 930.
[4] M. Radmacher, R. W. Tillmann, M. Fritz, H. E. Gaub, *Science* **1992**, *257*, 1900.
[5] M. Radmacher, M. Fritz, H. G. Hansma, P. K. Hansma, *Science* **1994**, *265*, 1577.
[6] D. T. Edwards, T. T. Perkins, *J. Struct. Biol.* **2017**, *197*, 13.
[7] V. S. Jadhav, D. Brüggeman, F. Wruck, M. Hegner, *Beilstein J. Nanotechnol.* **2016**, *7*, 138.
[8] M. Strackharn, S. W. Stahl, E. M. Puchner, H. E. Gaub, *Nano Lett.* **2012**, *12*, 2425.
[9] J. D. Pedelacq, S. Cabantous, T. Tran, T. C. Terwilliger, G. S. Waldo, *Nat. Biotechnol.* **2006**, *24*, 79.
[10] M. Strackharn, D. A. Pippig, P. Meyer, S. W. Stahl, H. E. Gaub, *J. Am. Chem. Soc.* **2012**, *134*, 15193.
[11] D. A. Pippig, F. Baumann, M. Strackharn, D. Aschenbrenner, H. E. Gaub, *ACS Nano* **2014**, *8*, 6551.
[12] S. F. Heucke, F. Baumann, G. P. Acuna, P. M. D. Severin, S. W. Stahl, M. Strackharn, I. H. Stein, P. Altpeter, P. Tinnefeld, H. E. Gaub, *Nano Lett.* **2013**, *14*, 391.
[13] S. Voss, A. Skerra, *Protein Eng.* **1997**, *10*, 975.
[14] F. Baumann, M. S. Bauer, L. F. Milles, A. Alexandrovich, H. E. Gaub, D. A. Pippig, *Nat. Nanotechnol.* **2016**, *11*, 89.
[15] J. Yin, P. D. Straight, S. M. McLoughlin, Z. Zhou, A. J. Lin, D. E. Golan, N. L. Kelleher, R. Kolter, C. T. Walsh, *Proc. Natl. Acad. Sci. USA* **2005**, *102*, 15815.
[16] H. Gumpp, S. W. Stahl, M. Strackharn, E. M. Puchner, H. E. Gaub, *Rev. Sci. Instrum.* **2009**, *80*, 063704.
[17] S. K. Kufer, E. M. Puchner, H. Gumpp, T. Liedl, H. E. Gaub, *Science* **2008**, *319*, 594.
[18] J. Morfill, K. Blank, C. Zahnd, B. Luginbühl, F. Kühner, K. E. Gottschalk, A. Plückthun, H. E. Gaub, *Biophys. J.* **2007**, *93*, 3583.
[19] W. Ott, M. A. Jobst, C. Schoeler, H. E. Gaub, M. A. Nash, *J. Struct. Biol.* **2016**, *197*, 3.
[20] U. Bockelmann, B. Essevaz-Roulet, F. Heslot, *Phys. Rev. Lett.* **1997**, *79*, 4489.
[21] R. Krautbauer, M. Rief, H. E. Gaub, *Nano Lett.* **2003**, *3*, 493.
[22] J. Morfill, F. Kühner, K. Blank, R. A. Lugmaier, J. Sedlmair, H. E. Gaub, *Biophys. J.* **2007**, *93*, 2400.
[23] C. Bustamante, J. F. Marko, E. D. Siggia, S. Smith, *Science* **1994**, *265*, 1599.
[24] E. A. Bayer, J. P. Belaich, Y. Shoham, R. Lamed, *Annu. Rev. Microbiol.* **2004**, *58*, 521.
[25] S. Moraïs, J. Stern, A. Kahn, A. P. Galanopoulou, S. Yoav, M. Shamshoum, M. A. Smith, D. G. Hatzinikolaou, F. H. Arnold, E. A. Bayer, *Biotechnol. Biofuels* **2016**, *9*, 164.
[26] J. Yin, A. J. Lin, D. E. Golan, C. T. Walsh, *Nat. Protoc.* **2006**, *1*, 280.
[27] J. L. Zimmerman, T. Nicolaus, G. Neuert, K. Blank, *Nat. Protoc.* **2010**, *5*, 975.
[28] E. Celik, V. T. Moy, *J. Mol. Recogn.* **2012**, *25*, 53.
[29] T. Hugel, M. Rief, M. Seitz, H. E. Gaub, R. R. Netz, *Phys. Rev. Lett.* **2005**, *94*, 048301.

